Partial cross sections and interfering resonances in photoionization of molecular nitrogen

Markus Klinker, Carlos Marante, Luca Argenti, Jesús González-Vázquez, and Fernando Martín

Phys. Rev. A **98**, 033413 — Published 18 September 2018

DOI: 10.1103/PhysRevA.98.033413

Partial Cross Sections and Interfering Resonances in the Photoionization of Molecular Nitrogen

Markus Klinker,[1,*] Carlos Marante,[1,†] Luca Argenti,[1,‡] Jesús González-Vázquez,[1] and Fernando Martín[1,2,3,§]

[1] *Departamento de Química, Módulo 13, Universidad Autónoma de Madrid, 28049 Madrid, Spain, EU*
[2] *Instituto Madrileño de Estudios Avanzados en Nanociencia (IMDEA-Nanociencia), Cantoblanco, 28049 Madrid, Spain, EU*
[3] *Condensed Matter Physics Center (IFIMAC), Universidad Autónoma de Madrid, 28049 Madrid, Spain, EU*

(Dated: August 27, 2018)

We present an in-depth theoretical study of N_2 photoionization in the region between the second ($^2\Pi_u$) and third ($^2\Sigma_u^+$) ionization thresholds. In this region, the electronic continuum includes the Hopfield series of autoionizing states, corresponding to excitations to $ns\sigma_d$, $nd\sigma_d$ and $nd\pi_g$ molecular orbitals. Calculations have been performed by using the XCHEM code, which makes use of a Gaussian/B-spline hybrid basis in the framework of a close-coupling approach. We provide total and partial photoionization cross sections for all open channels, energy positions and widths for the five lowest resonances of each series and, when resonances are well isolated from each other, Fano and Starace parameters. We also discuss how the coupling between the two series of overlapping resonances, $ns\sigma_d$ and $nd\sigma_d$, affects their energies and autoionization widths. These results show the potential of the XCHEM method to describe resonant photoionization in molecules.

I. INTRODUCTION

Advances in attosecond pulse generation have made possible the study of electron dynamics in molecules on extremely short time scales, yielding direct insight into how electronic rearrangement may affect chemical properties [1–5]. Inherent to these pulses are their high energy photons, as well as their broad spectra, allowing for ionization via absorption of a single photon and via multiple ionization channels, which when coupled lead to a very rich set of ultrafast processes, such as autoionization or Auger decay.

A necessary condition for any computational model aiming at studying these processes is the capability to describe, with high accuracy, the electronic continuum of the systems under investigation. This becomes extremely challenging with increasing size of the system, as the model must be able to represent both the intricate short range structure of complex molecular systems, as well as the long range nature of the continuum electron.

Existing methods, broadly speaking, deal with this difficulty in one of two ways. Either by employing methods specifically designed to provide a high level description of the long-range part of the electronic continuum, including autoionizing states, with the help of grid or pseudo-grid methods, or by partially disregarding, in one way or another, electron correlation [5]. For computational reasons, the former methods are difficult to generalize to systems beyond atomic or the simplest diatomic cases. Methods belonging to the second category allow one to describe ionization of relatively large molecules, but at a price: they are inherently incapable of describing autoionization and Auger decay.

Underpinning these limitations are the difficulties to merge existing computational methods that are able to provide an accurate description of electron correlation in molecular bound states (but cannot model continuum electrons) with those designed to represent scattering states in few-electron systems, which would be prohibitively expensive for normal molecules. The former, being the techniques of quantum chemistry, generally rely on an expansion of the wave function in terms of Gaussian basis functions, while the latter frequently rely on the use of compact-support functions such as B-splines [6–9] or discrete variable representations in combination with finite elements methods (FE-DVR) [10, 11]. More recently it has been shown that B-Splines can be used in combination with algebraic diagramatic construction (ADC) to obtain photoionization cross sections in atomic systems [12] and to study the effect of electron correlation in high harmonic generation [13]. Both, B-spline and FE-DVR based methods, have proven highly successful in their respective domains of application, due to the analytical simplicity of Gaussian functions and the flexibility of B-splines and FE-DVR at long range, but prove ill suited beyond it.

The XCHEM method has recently been proposed as an efficient way to merge the two approaches. It relies on a hybrid description of the wave function in terms of Gaussian functions and B-splines, allowing to overcome the problems associated with either type of function. The applicability of the XCHEM method in atomic and small diatomic benchmark systems has been well established [14, 15]. The next step is to apply the method to a poly-electronic molecular system. An excellent candidate is molecular Nitrogen, as it includes all the difficulties entailed by molecular scattering problems, while still being within the limits of what can be computed with existing methods, thus allowing us to make a com-

* markus.klinker@uam.es
† Present address: Lawrence Berkeley National Laboratory, 1 Cyclotron Rd, Berkeley, CA 94720, USA
‡ Present address: Department of Physics and CREOL College of Optics & Photonics, University of Central Florida, Orlando FL 32816, USA
§ fernando.martin@uam.es

parison. In a recent work by the authors [16] this was demonstrated for the total photoionization cross sections.

The complex continuum structure of Nitrogen has been experimentally studied for almost a century, yielding increasingly more accurate results with the availability of new light sources. Of particular interest has been the study of the ionization continuum between the second and third ionization thresholds, which was found to be strongly impacted by the presence of three series of autoionizing states, whose decay leaves the ionized molecule in either a $^2\Pi_u$ or $^2\Sigma_g^+$ state. Two of these series belong to the Σ_u^+ symmetry of the neutral state (which comprises both the ion and the ejected electron) and account for most of the structure seen in the photoionization spectrum. Experimentally these structures were first observed by Hopfield [17]. Ogawa and Tanaka [18] subsequently confirmed the existence of a third series. Since then a multitude of works have provided better resolution [19, 20], and investigated the relevance of vibration and rotation [21–23] and isotopic effects [24]. More recently time dependent measurements of the autoionization process have been carried out using an ionizing attosecond XUV pump pulse, alongside a delayed, IR femtosecond probe pulse [25]. In contrast with the abundance and history of experimental data available for the Hopfield series, their theoretical description has proven to be considerably more elusive due to the central role of correlation in the continuum states of this system. A few theoretical investigations of the autoionizing states in question, based on Multi Channel Quantum Defect Theory [26] and multichannel frozen-core Hartree-Fock approximation [27] do exist. However, they account for electron correlation only to a limited degree and rely on methods that do not easily scale to larger systems.

In this work we present the results obtained by using the XCHEM code and perform an in-depth analysis of the partial and total photoionization cross sections for molecular Nitrogen between the second and third ionization thresholds. As mentioned above, reference [16] has confirmed the accuracy of the total cross section by comparison with experiment and furthermore investigated the claims [28] of relevance of nuclear motion and non-adiabatic behavior. In the present work, we have extended these calculations to partial photoionization cross sections. We have extracted energy positions and widths for the five lowest resonances of each series and, when resonances are well isolated from each other, Fano and Starace parameters. We have also investigated the interaction between the two series of interfering resonances of Σ_u^+ symmetry. As suggested in [16], the strength of this interaction is mostly determined by electron correlation.

II. THEORY

The theoretical model used in this work is the XCHEM approach, introduced in references [14, 29]. The core idea of the XCHEM code is the combined use of: **a)** a close coupling expansion (CCE) of the molecular wavefunction $\Psi(\mathbf{x}_1, \cdots, \mathbf{x}_{\mathbf{N_e}})$, **b)** quantum chemistry (QC) methods exploiting the capabilities of commercial quantum chemistry packages (QCP) to describe the molecular short range structure, and **c)** a carefully designed set of basis functions comprised of Gaussians centered at the atomic sites, Gaussians centered at the molecular centre of mass (CoM) and B-Splines also centered at the CoM. The union of the latter two sets of basis functions is called a GABS basis and was introduced in reference [29]. Here we summarize how QCPs, CCE and GABS combine to achieve an accurate description of photoionization processes in molecular systems. For more information on the theoretical details of this method, as well as on its application to the photoionization of He, H_2 and Ne, which confirmed the viability of the XCHEM approach and motivated this work, we refer the reader to the past publications [14, 15].

A. XCHEM Approach

The construction of a molecular singly-ionized scattering function Ψ must account for the interaction of the short range structure of the molecular system, with the N_e^{th} electron liberated to the continuum. We begin by expanding Ψ in terms of a CCE

$$\Psi_{\alpha E}(\{\mathbf{x}\}_N) = \sum_i c_{i,\alpha E} \aleph_i(\{\mathbf{x}\}_N) + \sum_{\beta i} \left[N_{\beta i} \hat{\mathcal{A}} \Upsilon_\beta(\{\mathbf{x}\}_I; \hat{r}_{N_e}, \zeta_{N_e}) \phi_i(r_{N_e}) \right] c_{\beta i,\alpha E}, \quad (1)$$

where $\aleph_i$ denotes short range states with all electrons occupying the bound orbitals φ_{QC} obtained directly from QCPs, $\phi_i(r_{N_e})$ denotes the radial component of the electron ejected to the continuum, and Υ_β denotes the so called channel functions. The notation $\{\mathbf{x}\}_{N/I}$ refers to the set of all, or all but the last (the photoelectron's) electronic coordinates, respectively. Each term that appears in the sum over channel functions represents a single ionic molecular state Φ_b (with spin S_b and spin projection Σ_b) coupled to an electron with definite azimuthal and magnetic quantum numbers (l and m) to give rise to a state with total spin S and spin projection Σ,

$$\begin{aligned} \Upsilon_\beta(\{\mathbf{x}\}_I) &= {}^{2S+1}\left[\Phi_b(\{\mathbf{x}\}_I) \otimes \chi(\zeta_{N_e})\right]_\Sigma X_{lm}(\hat{r}_{N_e}) \\ &= \sum_{\Sigma_b \sigma} C^{S\Sigma}_{S_b\Sigma_b,\frac{1}{2}\sigma}\ {}^{2S_b+1}\Phi_{b,\Sigma_b}\ {}^2\chi_\sigma X_{lm}\ , \end{aligned} \quad (2)$$

where $C^{S\Sigma}_{S_b\Sigma_b,\frac{1}{2}\sigma}$ are Clebsch-Gordon coefficients, X_{lm} are symmetry-adapted spherical harmonics, and χ is the spin component of the N_e^{th} electron. Of all the terms appearing in the resulting expression for the molecular scattering state $\Psi_{\alpha E}$, only $\phi_i(r_{N_e})$ does not vanish at long radial range, whereas all the other terms, which account for complex many-body structures, are confined to a short distance from the CoM and are therefore susceptible to be

computed with QC methods, based on polycentric Gaussian (PCG) basis functions, centered at the atomic sites of the molecule. A similar treatment is not suitable for the radial component of the ejected electron, due to its non-decaying oscillatory character. To remedy this, the ejected electron is expanded in a GABS basis, which is characterized by two key parameters: **a)** the radius R_0 such that all B-Splines $B(r < R_0) = 0$, and **b)** the radius R_1 such that $R_1 > R_0$ and $|G^M(r > R_1)| << 1$, where G^M is any one of the monocentric Gaussian (MCG) basis functions contained in the GABS basis. It is assumed that all relevant QC orbitals (QCO) are negligible beyond R_0, $|\varphi_{\rm QC}(r > R_0, \hat{r})| << 1$. The following two paragraphs summarize how these assumptions facilitate the calculation of matrix elements between close-coupling states, as well as how multichannel scattering states fulfilling prescribed boundary conditions are obtained.

a. Matrix Elements: The antisymmetrized product on the second line of equation 1, referred to as extended-channel functions $\bar{\Upsilon}_{\alpha i}(\{\mathbf{x}_N\})$, may be created by augmenting the ionic states Φ_b, with an electron in one of three types of orbitals: **a**) Those created by the QCP, $\varphi_{\rm QC}$, which are expressed exclusively in terms of PCGs, **b**) monocentric orbitals (MCO), which are subsequently orthonormalized to the QCOs, and **c**) B-Spline orbitals. The strength of the XCHEM method becomes apparent in the computation of Hamiltonian matrix elements between augmented states. In the spatial region where short range interactions must be accounted for ($r < R_0$), the full wave function is expressed in terms of PCGs and MCGs, which allows us to compute matrix elements using standard tools already implemented in QCPs. Furthermore, by construction, an electron created in a B-spline orbital ϕ_j is guaranteed not to overlap with the short-range part of the wave function. As a consequence, when computing the matrix elements of any local operator $\hat{\mathcal{O}}$ between channel functions, with at least one resulting from augmentation with B-splines, the exchange term involving the last electron can be neglected [29]

$$\mathcal{O}_{\alpha i,\beta j} = \langle \bar{\Upsilon}_{\alpha i}|\hat{\mathcal{O}}|\bar{\Upsilon}_{\beta j}\rangle = \langle \Upsilon_\alpha \phi_i|\hat{\mathcal{O}}|\Upsilon_\beta \phi_j\rangle\,, \qquad (3)$$

where $\hat{\mathcal{A}}$ has disappeared in the last term.

b. Scattering States: From the matrix elements of the Hamiltonian in the close-coupling basis, it is possible to determine its stationary states. Bound states, with energy below the ionization thresholds, can be expressed in terms of a restricted close-coupling basis, in which the basis functions are required to vanish at the boundary of the quantization box. In this restricted basis, the Hamiltonian is Hermitian and can be directly diagonalized. Above the ionization thresholds, on the other hand, all energies are allowed, each energy is generally degenerate (there are as many states as the number of open channels) and the corresponding wave functions do not vanish at the box boundary. Still, these functions are essential to describe the physically relevant stationary collision regime in which an electron either approaches a parent ion or departs from it, having well described asymptotic quantum numbers, prior (outgoing boundary condition) and after (incoming boundary condition) the collision, respectively. Such scattering states are easily computed from the full set of eigenstates of the Hamiltonian confined to the box, together with their matrix elements with those close-coupling states that do not vanish at the box boundary. The procedure is described in detail in reference [14]. In a photoionzation process, the system is measured in terms of the quantum numbers of its fragments, after the interaction is over. Therefore such asymptotic states naturally fulfil the incoming boundary conditions. The corresponding scattering state has the following expression,

$$\Psi_{\alpha E} = \frac{1}{N_e}\sum N_{\beta E}\Upsilon_\beta \frac{u^-_{\beta,\alpha E}(r_{N_e})}{r_{N_e}}, \qquad (4)$$

where,

$$u^-_{\beta,\alpha E} = \delta_{\alpha\beta}\sqrt{\frac{2}{\pi k_\alpha}}e^{i\Theta_\alpha(r_{N_e})} - \sqrt{\frac{2}{\pi k_\beta}}e^{-i\Theta_\beta(r_{N_e})}\mathbb{S}^\star_{\beta\alpha}, \qquad (5)$$

where $\mathbb{S}$ denotes the scattering matrix and $\Theta_\alpha(r) = k_\alpha r + \frac{Z}{k_\alpha}\ln 2k_\alpha r - l_\alpha\pi/2 + \sigma_{l_\alpha}(k_\alpha)$, where k_α, Z and σ_{l_α} are the magnitude of the momentum of the ejected electron, the charge of the parent ion and the Coulomb phase, respectively [30]. Once the scattering states are found, it is possible to determine the asymptotic distribution of the photofragments of any wave packet. For example the photoionization cross section from the ground state of the system, Ψ_g, can be expressed as (we assume fixed orientation)

$$\sigma_{\alpha E} = \frac{4\pi^2}{c\omega}\left|\langle\Psi^-_{\alpha E}|\hat{\epsilon}\cdot\vec{P}|\Psi_g\rangle\right|^2 \qquad (6)$$

in velocity gauge, and

$$\sigma_{\alpha E} = \frac{4\pi^2\omega}{c}\left|\langle\Psi^-_{\alpha E}|\hat{\epsilon}\cdot\vec{R}|\Psi_g\rangle\right|^2, \qquad (7)$$

in length gauge, where $\hat{\epsilon}$ is the polarization of the ionizing light, and $\vec{P}/\vec{R}$ are the total canonical momentum and total electric dipole moment, respectively.

B. Quantum Chemistry

This section summarizes how QCPs may be extended to allow for the non-standard calculation of ionic states augmented with an electron expressed in an auxiliary set of MCGs. This is a crucial component of the XCHEM method, as it allows us to delegate all calculations involving intricate short-range structures to well-established QCPs (allowing treatment of systems of considerable complexity, subject only to the condition that the short range structure is confined within a radius R_0), while screening scattering calculations from this complexity. In this, and all previous works using the XCHEM

approach, the restricted-active-space self-consistent-field (RASSCF) method was used to express $\aleph$ and ${}^{2S_b+1}\Phi_{b\Sigma_b}$ as linear combinations of configuration-state functions (CSF), which are spin eigenfunctions, and may be related to linear combinations of slater determinants via the graphical unitary-group approach (GUGA). Creation of neutral states via augmentation of ${}^{2S_b+1}\Phi_{b\Sigma_b}$ with a further electron, translates to the application of the creation operator $\hat{a}_i^\dagger$, where i denotes MCG orbitals and the PCG orbitals φ_{QC} contained in the active space. We deliberately exclude virtual orbitals, as they generally do not comply with the condition $|\varphi_{\mathrm{QC}}(r > R_0, \hat{r})| << 1$, unless an impractically large R_0 is chosen. Application of $\hat{a}_i^\dagger$ is easily done in the determinantal expansion of ${}^{2S_b+1}\Phi_{b\Sigma_b}$.

It is important to note that $\hat{a}_i^\dagger\ {}^{2S_b+1}\Phi_{b\Sigma_b}$ may not have definite spin, in which case the components of the augmented states with the desired spin are recovered by reverting to a description in terms of CSFs, via use of the appropriate GUGA table for the augmented system.

From a computational perspective, two points are worth making. The combination of PCGs and MCGs in QCPs leads to large basis sets. On the other hand, to describe singly-ionized states, only bielectronic integrals with at most two MCG indeces are needed. Thanks to this latter circumstance, it is possible to drastically reduce the computational effort of the SEWARD integral module of the MOLCAS package. The computational cost of computing matrix elements between single-ionization augmented states is also similarly reduced, since for all CSFs contributing to these states at most one MCG orbital is occupied by at most one electron.

III. RESULTS

We investigate the three Hopfield series of autoionizing states lying between the second (${}^2\Pi_u$) and third (${}^2\Sigma_u^+$) ionization thresholds. Of these series, one is of ${}^1\Pi_u$ symmetry while the other two are of ${}^1\Sigma_u^+$ symmetry. The former series corresponds to a non-valence excitation from the $2\sigma_u$ orbital to an $nd\pi_g$ orbital, whereas the latter two correspond to non-valence excitations from the same orbital to $ns\sigma_g$ and $nd\sigma_g$ orbitals, respectively. Upon excitation, the states in the series of ${}^1\Pi_u$ symmetry couple to the continuum via five open channels; three of which (ejecting $\varepsilon s\sigma_g$, $\varepsilon d\sigma_g$ and $\varepsilon d\delta_g$ electrons) leave the ionic system in the ${}^2\Pi_u$ state and two of which (ejecting $\varepsilon p\pi_u$ and $\varepsilon f\pi_u$ electrons) leave the ionic system in the ${}^2\Sigma_g^+$ state. Conversely, the states in the two series of ${}^1\Sigma_u^+$ symmetry may autoionize by coupling to the following three continuum channels: ejecting a $\varepsilon d\pi_g$ electron leaving the ionic system in the ${}^2\Pi_u$ state, or ejecting a $\varepsilon p\sigma_u$ or $\varepsilon f\sigma_u$ electron leaving the ionic system in the ${}^2\Sigma_g^+$ state. In the CCE (equation 1), a total of eleven channels have to be included, eight of which are open, in the energy region of interest. Figure 1 illustrates the relevant channels, the three series of autoionizing states, and how they couple to the continuum.

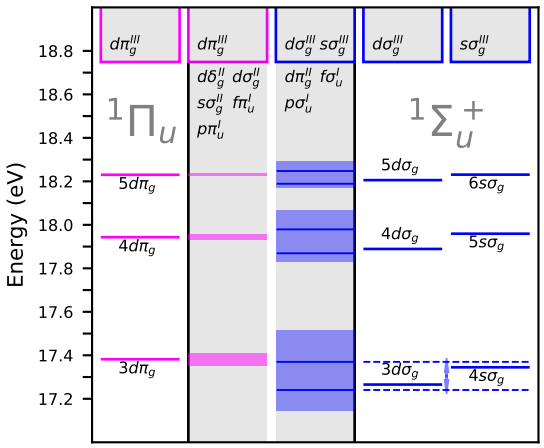

FIG. 1. Open and closed channels between the second and third ionization thresholds, included in the present calculation. The white columns indicate the closed channels, with the autoionizing states of Π_u symmetry (magenta) and Σ_u^+ (blue). The grey columns correspond to open channels, with the symmetries of the ejected electrons indicated in each, and whose superscripts denote the associated ionized molecule, i.e. ${}^2\Sigma_g^+$ (I), ${}^2\Pi_u$ (II) or ${}^2\Sigma_u^+$ (III). The coloured bars within the open channels indicate the effect of coupling the available (open and closed) channels on the autoionizing states: they acquire width, and in the case of the two series of Σ_u^+, experience a change in position (schematically indicated for the lowest pair of autoionizing states) due to a coupling of the two series to each other.

In order to represent the aforementioned channels accurately, the QC calculations were carried out using the cc-pVQZ [31] basis set (acting as the PCG basis) in a State Averaged Restricted Active Space Self Consistent Field Theory (SA-RASSCF) calculation. The active space used has the following specifications: doubly occupied (closed) $1\sigma_{g/u}$ orbitals, all possible excitation (complete active space) in $2\sigma_{g/u}$, $3\sigma_{g/u}$ and $1\pi_{g/u}$ orbitals, and single and double excitations (restricted active space) in $4\sigma_{g/u}$, $5\sigma_{g/u}$, $6\sigma_{g/u}$, $2\pi_{g/u}$, $3\pi_{g/u}$ and $1\delta_{g/u}$ orbitals (where in this notation the number indicates the energetic ordering of the orbitals within a given symmetry). The orbitals were optimized over a State Average that comprises the $X^1\Sigma_g^+$, $A^1\Pi_u$, $B^1\Pi_u$, and $C^1\Sigma_u^+$ neutral states. This choice yielded the best simultaneous description of the relevant neutral (i.e. the ground state) and ionic states. To allow a State Average calculation over states of different symmetry, the QCP Molpro [32] was used. The remaining steps of the XCHEM method, namely the augmentation of the ionic states in the MCG basis, and the subsequent evaluation of matrix elements, were carried with the QCP MOLCAS [33]. Apart from augmentation in the active QCOs directly obtained from QCPs, neutral states were calculated by augmenting in MCOs obtained from an even tempered MCG basis con-

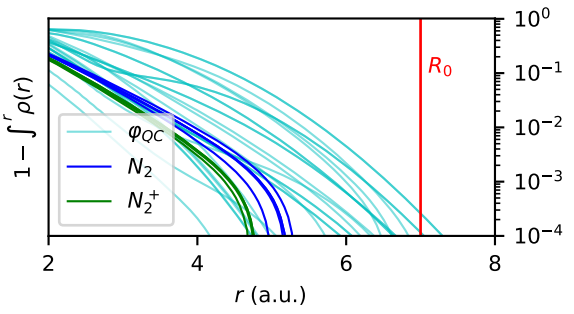

FIG. 2. Radial behavior of the integrated electron density of all quantities expressed in PCGs: the short range states $\aleph$ (blue lines), the ionic states Φ (green lines) and the active QCOs $\varphi_{\rm QC}$ (cyan lines), in which the ionic states are augmented. The red line marks the chosen R_0. It is evident, that all PCG-depended quantities are confined well within this radius, and thus the assumption of zero overlap between the B-splines and the PCGs is justified.

taining radial functions of the type $G_{ikl} \propto r^{l+2k}e^{-\alpha_i r^2}$, with $i = 0\cdots 21$ defining the exponents as $\alpha_i = \alpha_0\beta^i$ where $\alpha_0 = 0.001$ and $\beta = 1.46$, $k \leq 2$ and $l \leq 3$. With these parameters it is possible to set R_0 well beyond the active QC/PCG range without compromising the matching between B-splines and MCG orbitals. To justify the choice of R_0 in the present case, figure 2 shows the dependence on the radius r of the angularly integrated electron density of all quantities whose description in terms of PCGs we rely on. From the figure it is obvious that $R_0 = 7.0$ a.u. is sufficiently large to avoid significant protrusion of PCGs beyond R_0. The remaining parameter defining the B-spline basis are $R_{\rm max} = 200$ a.u., number of B-spline: 390, order of B-spline: 7.

Figure 3 shows the total photoinoization cross section, as well as the individual contributions arising from the Π_u channels and the Σ_u^+ channels, in length and velocity gauge. The gauge agreement (especially for Σ_u^+) is very good. Reference [16] confirmed the high level of accuracy of these results when compared to experimental data, with the exception of the lowest resonance feature ($n = 3$) in the Σ_u^+ channel (the resonance labels in figure 3 follow the notation of reference [26]). Let us now examine the series of autoionizing states in each symmetry separately. The main qualitative difference between them is that, whereas in Π_u symmetry all visible features are attributable to a single series ($nd\pi_g$) of well separated resonances, in Σ_u^+ symmetry, both the $ns\sigma_g$ and $nd\sigma_g$ series, which overlap, contribute to the spectrum. The letter case therefore requires a more elaborate analysis. For this reason we shall begin the investigation with the more straightforward case of the $nd\pi_g$ series.

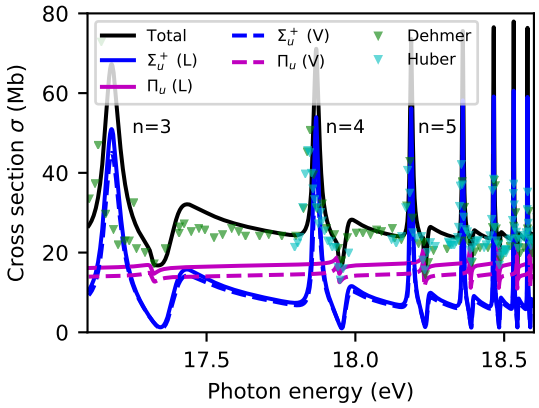

FIG. 3. Photoionization cross sections (CS) between the second and third ionization threshold of N_2. Continuous lines correspond to length gauge and dashed lines to velocity gauge. The total CS is shown in black, while the contributions leaving the system in a Σ_u^+ or Π_u state are shown in blue and magenta, respectively. The former exhibits resonance features corresponding to the series of $ns\sigma_g$ and $nd\sigma_g$ autoionizing states, while the latter exhibits the (much less pronounced) resonance features of the $np\pi_u$ series of autoionizing states. Symbols show the experimental results of Dehmer [22] and Huber [23].

A. Π_u Autoionizing States

Figure 4b shows the breakdown of the photoionization cross section into its partial components, corresponding to decay to any one of the five open channels for this symmetry. The shape of the resonances aside, the branching ratios to the different channels are approximately constant with energy, with the $d\delta_g$ channel being dominant (and responsible for the bulk of the resonance features), and the probability of leaving a $^2\Pi_u$ ion behind being roughly twice that of the ionic ground state ($^2\Sigma_g^+$). Furthermore, for all channels, the presence of autoionizing states only weakly attenuates the background. Figure 4a shows the phase shift of the final scattering state, which exhibits characteristic π jumps in the vicinity of autoionizing states.

These resonances have been analized following the parametrization proposed by Fano [34, 35], as well as investigating the eigenphase sum near resonances [36]. The positions (E^r) and widths (Γ) of the autoionizing states may be obtained in a straightforward manner by using the following expression, which relates E^r and Γ to the resonant part of the scattering phase shift ϕ^r:

$$\tan(\phi^r) = \frac{\Gamma/2}{E^r - E}. \tag{8}$$

Once the energy and width have been fixed, we may extract the Fano parameter q and correlation parameter ρ^2 by fitting the total cross section to the analytical expression describing the, characteristically asymmetric,

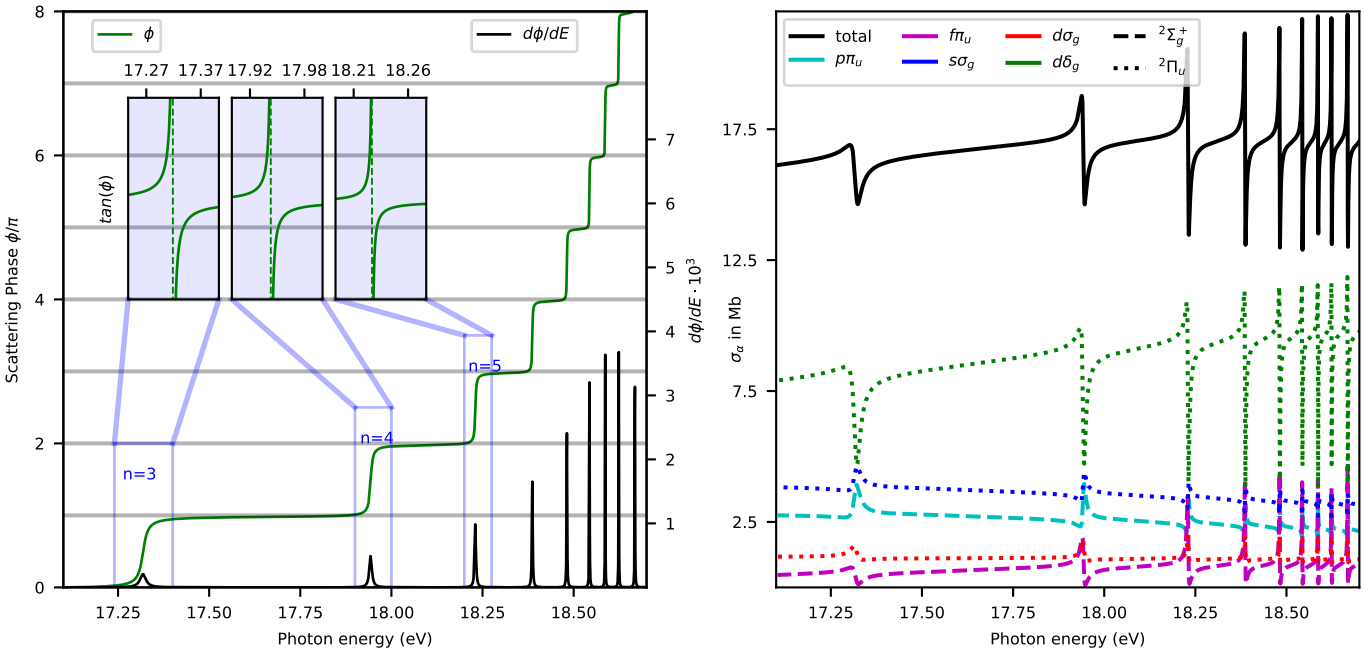

FIG. 4. (a) Phase shift (green curve) of scattering states of Π_u symmetry. Clearly observable are the pronounced π - phase jumps as the photon energy scans across autoionizing states (Furthermore it may be noted that in this case the background is practically flat). Also shown is the tangents of the scattering phase shift (in the inlets) for the first three resonance features, whose poles (dashed vertical lines) yield the positions E^r, and the derivative of ϕ^r (black curve), the value of which at E^r allows calculation of the widths Γ. (b) The total (full black curve) and partial (dashed and dotted curves) photoionization cross sections of channels with photo electrons $p\pi_u$, $f\pi_u$, $s\sigma_g$, $d\sigma_g$ and $d\delta_g$ (shown here only in length gauge). The resonances are evidently well separated in energy and appear as individual (characteristically asymmetric) Fano peaks. The dashed and dotted patterns indicate if the ionic molecule is found in a $^2\Sigma_g^+$ state or $^2\Pi_u$ state, respectively.

resonance shape in the presence of several open channels:

$$\sigma(E) = \sigma_b(E)\left[\frac{\rho^2(q+\varepsilon)^2}{\varepsilon^2+1} + 1 - \rho^2\right], \tag{9}$$

where ε is the reduced energy given by $\varepsilon = 2(E-E^r)\Gamma^{-1}$. The results are summarized in the upper part of table I, with values obtained in length and velocity gauge for q and ρ^2. While there is a notable quantitative difference for q in the two gauges, the agreement is very good for ρ^2. Having fixed the parameters characterizing the total cross section, the corresponding parameters for the resonance features appearing in the partial cross sections (of figure 4), for a specific channel α with an electron of given angular momentum being ejected, can be extracted by fitting to the slightly more involved expression [37], valid for the partial photoionization cross sections:

$$\sigma_\alpha(E) = \frac{\sigma_{b,\alpha}(E)}{\varepsilon^2+1}\left(\varepsilon^2 + 2\varepsilon\left[q\mathrm{Re}(\rho_\alpha) - \mathrm{Im}(\rho_\alpha)\right] + 1 - 2\left[q\mathrm{Im}(\rho_\alpha) + \mathrm{Re}(\rho_\alpha)\right] + |\rho_\alpha|^2(q^2+1)\right), \tag{10}$$

where ρ_α is the so called Starace parameter, which may be understood as a complex extension of the correlation parameter ρ^2 of equation 9, and whose real and imaginary part enter as parameters in the fitting procedure. Apart from the large number of parameters, the fitting is now further complicated by the fact that the Starace parameters for the different channels fulfil

$$\sum_\alpha \sigma_{b,\alpha}|\rho_\alpha|^2 = \sigma_b|\rho|^2. \tag{11}$$

An alternative parametrization for the partial photoionization cross sections can be obtained by using the expression [38]:

$$\sigma_\alpha = \frac{\sigma_{b,\alpha}(E)}{\varepsilon^2+1}(\varepsilon^2 + C_{1,\alpha}\varepsilon + C_{2,\alpha}). \tag{12}$$

The parameters $C_{1,\alpha}$ and $C_{2,\alpha}$ may be used to evaluate the Starace parameter via a different route, and thus, give credence to the extracted values, by verifying the

expressions:

$$\mathrm{Re}(\rho_\alpha) = \frac{qC_{1,\alpha} + 2 \pm \sqrt{4C_{2,\alpha} - C_{1,\alpha}^2}}{2(1+q^2)}$$
$$\mathrm{Im}(\rho_\alpha) = \frac{q\left(2 \pm \sqrt{4C_{2,\alpha} - C_{1,\alpha}^2}\right) - C_{1,\alpha}}{2(1+q^2)}$$
$$4C_{2,\alpha}^2 \geq C_{1,\alpha}^2, \tag{13}$$

relating the two parametrizations of the partial cross sections (the last expression ensures that $\mathrm{Re}(\rho_\alpha)$ and $\mathrm{Im}(\rho_\alpha)$ are themselves real).

We obtained the values for either parametrization by fitting the relevant formulas to the calculated cross sections. The values are presented in the lower part of table I. For the $p\pi_u$ channel results for both, length and velocity gauge are included, and are seen to be in good agreement.

B. Σ_u^+ Autoionizing States

Figure 5b shows the total and partial photoionization cross sections of the relevant channels in Σ_u^+ symmetry. Here, the impact of the autoionizing states on the background cross sections, as well as the qualitative difference between the different channels, are more pronounced than in Π_u symmetry, as the dramatic dependence of the branching ratios on the photon energy shows. Most notably, for every n we observe an energy at which only one channel (ejected electron: $p\sigma_u$, ionic molecule: $^2\Sigma_g^+$), has a non-zero cross section, accompanied furthermore by a significant reduction in the total cross section.

We shall begin the quantitative analysis in much the same way as for the previous section; by obtaining the positions and widths of the autoionizing states, by looking at the jumps undergone by the scattering phase (shown in figure 5a). While this was essentially trivial in the previous case, the situation here is somewhat more involved, as one must now account for the fact that the resonances appearing for each n in both series are energetically very close. Thus, we have performed a very fine scan in photon energies and fitted every couple of s and d resonances to the sum of two terms as given in equation 8. The resulting energy positions and widths (now denoted $E_\pm$ and $\Gamma_\pm$ for the reasons explained below) are given in the first two rows of table II. For the higher members of the series ($n > 3$), these values are slightly different from those reported in [16] due to the finer scan of photon energies used in the present work.

As the members of the two series of autoionizing states are energetically closer than their combined widths, the individual states couple not only to the continuum states, but may also couple to each other, either directly or via the available continua. The effect of this has been the subject of several works [39–44], and results in the resonance positions and width being modified compared to what would be observed in the absence of coupling between them. These modified positions correspond to the energies $E_\pm$ presented in table II (schematically also shown for $n = 3$ in figure 1), and are the ones observable in experiment.

While interesting in their own right, $E_\pm$ and $\Gamma_\pm$ once obtained do not yet allow us to make any statement about the possible impact of the coupling of the two series of autoionizing states to each other. In order to do

α		$n=3$	4	5	6	7
Total Photoionization Cross Section						
	E^r (eV)	17.318	17.943	18.230	18.387	18.481
	Γ (meV)	19.3	8.2	4.0	2.3	1.4
	q_L	−0.57	−0.86	−0.97	−1.02	−1.04
	q_V	−0.79	−1.11	−1.09	−1.12	−1.15
	ρ_L^2	0.105	0.141	0.213	0.234	0.242
	ρ_V^2	0.099	0.136	0.206	0.228	0.236
Partial Photoionization Cross Section						
$p\pi_u$	$\mathrm{Re}(\rho_\alpha)_L$	−0.182	−0.215	−0.161	−0.150	−0.150
	$\mathrm{Re}(\rho_\alpha)_V$	−0.171	−0.208	−0.156	−0.146	−0.146
	$\mathrm{Im}(\rho_\alpha)_L$	−0.017	−0.047	−0.067	−0.069	−0.072
	$\mathrm{Im}(\rho_\alpha)_V$	−0.016	−0.046	−0.065	−0.067	−0.070
	$C_{1,\alpha,L}$	0.243	0.464	0.445	0.443	0.458
	$C_{1,\alpha,V}$	0.301	0.552	0.469	0.461	0.476
	$C_{2,\alpha,L}$	1.388	1.435	1.251	1.215	1.207
	$C_{2,\alpha,V}$	1.366	1.415	1.234	1.200	1.192
$f\pi_u$	$\mathrm{Re}(\rho_\alpha)$	0.577	0.845	0.893	0.949	0.970
	$\mathrm{Im}(\rho_\alpha)$	0.241	0.418	0.768	0.832	0.849
	$C_{1,\alpha}$	−1.143	−2.290	−3.265	−3.592	−3.719
	$C_{2,\alpha}$	0.642	1.576	3.389	4.027	4.294
$s\sigma_g$	$\mathrm{Re}(\rho_\alpha)$	−0.100	−0.105	−0.080	−0.071	−0.069
	$\mathrm{Im}(\rho_\alpha)$	−0.021	−0.048	−0.067	−0.072	−0.075
	$C_{1,\alpha}$	0.156	0.276	0.288	0.288	0.292
	$C_{2,\alpha}$	1.190	1.150	1.052	1.016	1.003
$d\sigma_g$	$\mathrm{Re}(\rho_\alpha)$	−0.016	−0.008	0.006	0.010	0.012
	$\mathrm{Im}(\rho_\alpha)$	0.190	0.241	0.272	0.280	0.287
	$C_{1,\alpha}$	−0.363	−0.468	−0.556	−0.581	−0.599
	$C_{2,\alpha}$	1.298	1.531	1.660	1.708	1.748
$d\delta_g$	$\mathrm{Re}(\rho_\alpha)$	0.228	0.247	0.305	0.319	0.325
	$\mathrm{Im}(\rho_\alpha)$	0.004	0.010	0.015	0.015	0.016
	$C_{1,\alpha}$	−0.270	−0.446	−0.621	−0.679	−0.709
	$C_{2,\alpha}$	0.618	0.630	0.599	0.600	0.605

TABLE I. The parameters characterizing the total and partial photoionization cross sections of the $nd\pi_u$ Hopfield series. For the partial cross sections the results for both paramterizations (equations 10 and 12) are given, where it is trivial to ascertain that, upon insertion in equation 13, the two are consistent. The subscrips indicate (L)ength and (V)elocity gauge. If no subscript is present, length gauge is implied.

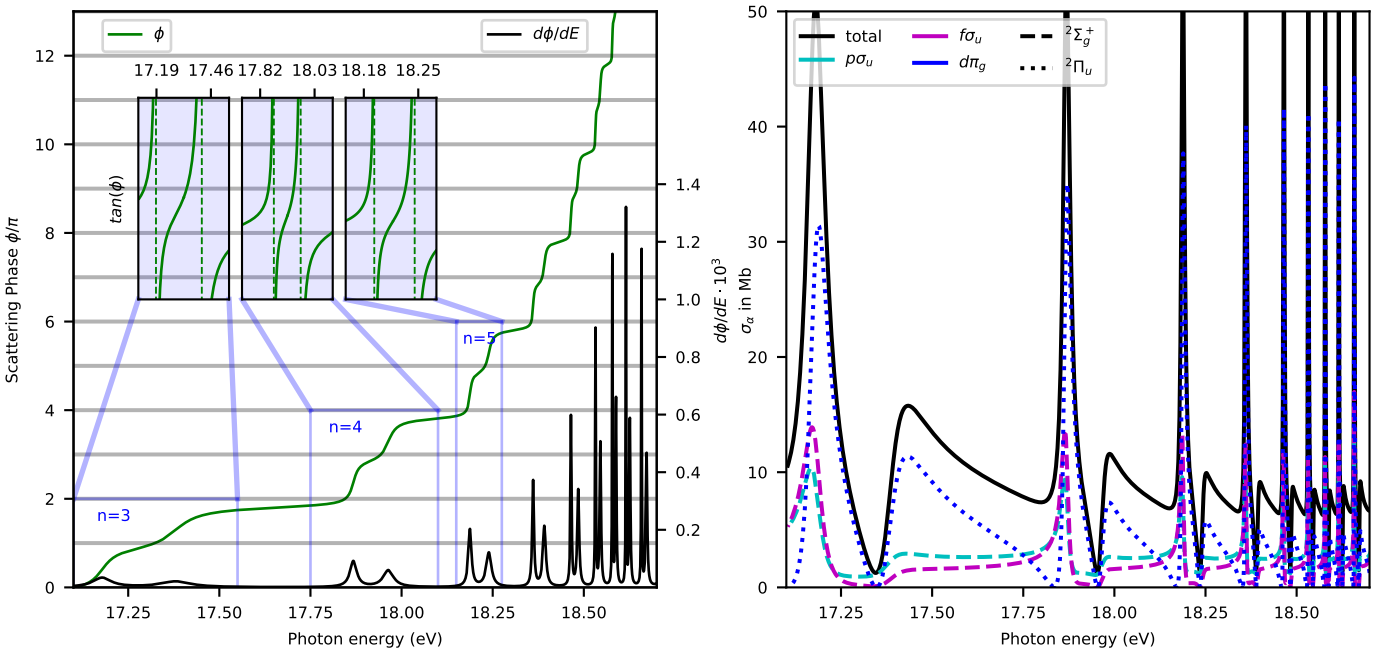

FIG. 5. (a) Phase (green curve) of scattering states of Σ_u symmetry. Clearly observable are the pronounced pairs of π - phase jumps as the photon energy scans across pairs of autoionizing states of the $ns\sigma_d$ and $nd\sigma_g$ series. Also shown is the tangents of the scattering phase (in the inlets) for the first three resonance features. (b) The total (full black curve) and partial (dashed and dotted curves) photoionization cross sections of channels with photo electrons $p\sigma_u$, $f\sigma_u$, and $d\pi_g$ (shown here only in length gauge). In sharp contrast to figure 4, the two features appearing for every n are not well separated, and the possibility of coupling between them must be accounted for. Furthermore it is noteworthy that, in the valley after the more pronounced peak visible in the resonance feature for each n, we observe the presence of a photon energy at which the electron is exclusively emitted as a $p\sigma_u$ electron. This also implies that, at these energies, the ionized molecule is found exclusively in a $^2\Sigma_g^+$ state, as indicated by the dashed or dotted pattern, analogous to figure 4.

$n=$	3		4		5		6		7	
E_-, E_+ (eV)	17.171	17.388	17.866	17.966	18.187	18.240	18.360	18.392	18.465	18.485
E_d, E_s (eV)	17.265	17.345	17.933	17.943	18.210	18.222	18.370	18.380	18.470	18.477
Γ_+, Γ_- (meV)	62.8	98.2	23.0	34.1	10.1	16.8	5.5	9.5	3.3	5.9
Γ_d, Γ_s (meV)	43.6	165.6	9.5	72.2	6.8	30.8	4.2	15.4	2.7	8.8

TABLE II. The energies and widths of the $ns\sigma_g$ and $nd\sigma_g$ series. $E_\pm$ are the true resonance position, whereas $E_{s,d}$ are the energies disregarding the interference between the two series (analogous for the widths Γ). The difference between the two sets of results is attributable to the strength of the coupling between the two series, resulting in the resonances being pushed apart, and the widths Γ_+ increasing at the expense of Γ_-.

so, knowledge of the resonance positions $E_{s/d}$, neglecting the coupling between the corresponding autoionizing states, is necessary (the corresponding widths are analogously denoted by $\Gamma_{s/d}$). If there is a significant discrepancy between $E_{s/d}$ and $E_\pm$ (as well as $\Gamma_{s/d}$ and $\Gamma_\pm$) we can conclude that interference between autoionzing states plays an important role in this system. We may obtain values for $E_{s/d}$ and $\Gamma_{s/d}$ by carrying out a separate calculation that disregards the coupling between the channels containing the $ns\sigma_g$ and $nd\sigma_g$ states (i.e. the two rightmost channels in figure 1). In terms of the XCHEM approach this translates to two separate calculations, excluding from the MCOs and B-splines either $s\sigma_g$ orbitals or $d\sigma_g$ orbitals, respectively. The bottom two rows of table II show the values obtained from these calculations

Comparing the results for the coupled and decoupled case in table II, we observe that the coupling between the two series causes the resonances to be pushed apart as well as the widths Γ_s and Γ_d decreasing and increasing, respectively. Thus we may unambiguously conclude, that a correct description of the Hopfield $s\sigma_g$ and $d\sigma_g$ series of autoionizing states necessarily requires that the coupling of its members to each other be included in the calculation.

IV. CONCLUSIONS AND OUTLOOK

We have shown that the XCHEM method, relying on a hybrid basis of Gaussian and B-spline functions is able to provide an accurate description of the electronic continuum of Nitrogen between the second and the third ionization thresholds, where electron correlation plays a very important role and a multitude of resonances associated with the presence of autonization states is observed. This work represents the first application of the XCHEM code to a molecular system, for which scattering states are not easily accessible by comparable alternative methods. This is an important step forward, as most of the challenges the XCHEM sets out to overcome do not manifest themselves in simple systems containing very few electrons. Specifically the multi-centered nature of the basis functions inherent in this approach, with Gaussian functions at the atomic sites and Gaussian and B-spline functions at the centre of mass, has now conclusively been shown to allow for a seamless and scalable merging of the tools of scattering theory and quantum chemistry. Furthermore the unprecedented number of CSFs used here to optimize the molecular orbitals, of the order of magnitude of 10^6, demonstrates the possibility to harnessing the power of quantum chemistry in molecular photoionization problems.

Taking advantage of the new possibilities offered by the XCHEM code, we have performed a detailed analysis of the Hopfield series of autoionizing states. This includes obtaining the energies and widths of the three series of autoionizing states lying in this region of the electronic continuum. We have also extracted the Fano parameters q and ρ^2 characterizing resonant peaks in the total photoionization cross section and the Starace parameters for the corresponding peaks in the partial photoionization cross sections of the five channels associated with the $nd\pi_g$ series. To the best of our knowledge, only the energy positions and widths have previously been reported in literature. Furthermore we have shown, by using a secondary set of XCHEM calculations, the importance of the coupling between the overlapping members of the $ns\sigma_d$ and $nd\sigma_g$ series.

All the above establishes the XCHEM method as an excellent candidate for the study of even larger molecular systems to a similar level of theory, thereby going firmly beyond what is possible with current methods. Systems readily accessible with the current XCHEM methodology are, e.g., water and pyrazine. A further avenue of investigation, especially given the interest in the processes mentioned in the introduction, is to use the results of the XCHEM code to solve the time dependent Schrödinger Equation. This is currently being undertaken in our group.

V. ACKNOWLEDGEMENTS

This work has been supported by the ERC advanced grant 290853 - XCHEM - within the seventh framework programme of the European Union, the ERC proof-of-concept grant 780284 - Imaging-XChem - within the Horizon2020 Framework Programme, and the MINECO project FIS2016-77889-R (AEI/FEDER, UE). We also acknowledge computer time from CCC-UAM and Marenostrum Supercomputer Centers. L.A. acknowledges support from the TAMOP NSF Grant No. 1607588, as well as UCF funding.

[1] F. Krausz and M. Ivanov, Rev. Mod. Phys. **81**, 163 (2009).
[2] G. Sansone, F. Kelkensberg, J. F. Pérez-Torres, F. Morales, M. F. Kling, W. Siu, O. Ghafur, P. Johnsson, M. Swoboda, E. Benedetti, F. Ferrari, F. Lépine, J. L. Sanz-Vicario, S. Zherebtsov, I. Znakovskaya, a. L @ YHuillier, M. Y. Ivanov, M. Nisoli, F. Martín, and M. J. J. Vrakking, Nature **465**, 763 (2010).
[3] F. Calegari, D. Ayuso, A. Trabattoni, L. Belshaw, S. De Camillis, S. Anumula, F. Frassetto, L. Poletto, A. Palacios, P. Decleva, J. B. Greenwood, F. Martín, and M. Nisoli, Science **346**, 336 (2014).
[4] P. M. Kraus, B. Mignolet, D. Baykusheva, A. Rupenyan, L. Horný, E. F. Penka, G. Grassi, O. I. Tolstikhin, J. Schneider, F. Jensen, L. B. Madsen, A. D. Bandrauk, F. Remacle, and H. J. Wörner, Science **350**, 790 (2015).
[5] M. Nisoli, F. Calegari, A. Palacios, P. Decleva, and F. Martín, Chem. Rev. **117**, 10760 (2017).
[6] I. Sánchez and F. Martín, The Journal of chemical physics **106**, 7720 (1997).
[7] F. Martín, Journal of Physics B: Atomic, Molecular and Optical Physics **32**, R197 (1999).
[8] Y. V. Vanne, A. Saenz, A. Dalgarno, R. C. Forrey, P. Froelich, and S. Jonsell, Physical Review A **73**, 062706 (2006).
[9] W. Vanroose, D. A. Horner, F. Martin, T. N. Rescigno, and C. W. McCurdy, Physical Review A **74**, 052702 (2006).
[10] T. N. Rescigno and C. W. McCurdy, Physical review A **62**, 032706 (2000).
[11] L. Tao, C. W. McCurdy, and T. N. Rescigno, Physical Review A **82**, 023423 (2010).
[12] M. Ruberti, V. Averbukh, and P. Decleva, The Journal of chemical physics **141**, 164126 (2014).
[13] M. Ruberti, P. Decleva, and V. Averbukh, Physical Chemistry Chemical Physics **20**, 8311 (2018).
[14] C. Marante, M. Klinker, I. Corral, J. González-Vázquez, L. Argenti, and F. Martín, Journal of Chemical Theory and Computation **13**, 499 (2017).
[15] C. Marante, M. Klinker, T. Kjellsson, E. Lindroth, J. González-Vázquez, L. Argenti, and F. Martín, Phys. Rev. A **96**, 022507 (2017).
[16] M. Klinker, C. Marante, L. Argenti, J. González-Vázquez, and F. Martín, The journal of physical chemistry letters **9**, 756 (2018).

[17] J. J. Hopfield, Phys. Rev. **35**, 1133 (1930).
[18] M. Ogawa and Y. Tankaka, Canadian Journal of Chemistry **40**, 1593 (1962).
[19] P. Gürtler, V. Saile, and E. E. Koch, Chemical Physics Letters **48**, 245 (1977).
[20] A. C. Parr, D. L. Ederer, B. E. Cole, J. B. West, R. Stockbauer, K. Codling, and J. L. Dehmer, Physical Review Letters **46**, 22 (1981).
[21] P. R. Woodruff and G. V. Marr, Proceedings of the Royal Society A **358**, 87 (1977).
[22] M. P. Dehmer, P. J. Miller, and W. A. Chupka, The Journal of Chemical Physics **80**, 1030 (1984).
[23] K. P. Huber, G. Stark, and K. Ito, The Journal of Chemical Physics **98**, 4471 (1993).
[24] J. B. Randazzo, P. Croteau, O. Kostko, M. Ahmed, and K. A. Boering, J. Chem. Phys. **140**, 194303 (2014).
[25] M. Reduzzi, W. C. Chu, C. Feng, A. Dubrouil, J. Hummert, and F. Calegari, Journal of Physics B **49**, 0 (2016).
[26] M. Raoult, H. Le Rouzo, G. Raseev, and L. H. Brion, Journal of Physics B **16**, 4601 (1983).
[27] R. R. Lucchese and R. W. Zurales, Physical Review A **44**, 291 (1991).
[28] M. Eckstein, C.-H. Yang, F. Frassetto, L. Poletto, G. Sansone, M. J. J. Vrakking, and O. Kornilov, Physical Review Letters **116**, 163003 (2016).
[29] C. Marante, L. Argenti, and F. Martín, Physical Review A **90**, 012506 (2014).
[30] R. G. Newton, *Scattering theory of waves and particles* (Springer Science & Business Media, 2013).
[31] T. H. Dunning Jr, The Journal of chemical physics **90**, 1007 (1989).
[32] H.-J. Werner, P. J. Knowles, G. Knizia, F. R. Manby, and M. Schütz, Wiley Interdisciplinary Reviews: Computational Molecular Science **2**, 242 (2012).
[33] F. Aquilante, J. Autschbach, R. K. Carlson, L. F. Chibotaru, M. G. Delcey, L. De Vico, N. Ferré, L. M. Frutos, L. Gagliardi, and M. Garavelli, Journal of computational chemistry **37**, 506 (2016).
[34] U. Fano, Physical Review **124**, 1866 (1961).
[35] U. Fano and J. W. Cooper, Physical Review **137**, A1364 (1965).
[36] A. U. Hazi, Physical Review A **19**, 920 (1979).
[37] A. F. Starace, Physical Review A **16**, 231 (1977).
[38] L. Journel, B. Rouvellou, D. Cubaynes, J. Bizau, F. Wuilleumier, M. Richter, P. Sladeczek, K.-H. Selbmann, P. Zimmermann, and H. Bergeron, Le Journal de Physique IV **3**, C6 (1993).
[39] F. H. Mies, Physical Review **175**, 164 (1968).
[40] L. Davis and L. Feldkamp, Physical Review B **15**, 2961 (1977).
[41] H. Friedrich and D. Wintgen, Physical Review A **32**, 3231 (1985).
[42] P. Durand and I. Paidarova, Journal of Physics B: Atomic, Molecular and Optical Physics **35**, 469 (2002).
[43] A. I. Magunov, I. Rotter, and S. I. Strakhova, Physical Review B **68**, 245305 (2003).
[44] M. Tabanli, J. Peacher, and D. H. Madison, Journal of Physics B: Atomic, Molecular and Optical Physics **36**, 217 (2003).